Enhanced Teleoperation Performance Using Hybrid Control and Virtual Fixture

Jing Luo[a], Chenguang Yang[b,⋆], Ning Wang[c,d], and Min Wang[a]

[a]Key Laboratory of Autonomous Systems and Networked Control, College of Automation Science and Engineering, South China University of Technology, Guangzhou, 510640 China;
[b]Bristol Robotics Laboratory, UWE Bristol, BS16 1QY, UK;
[c] Centre for Robotics and Neural Systems, Plymouth University, PL4 8AA, UK;
[d] School of Information Engineering, Chang'an University, Middle-section of Nan'er Huan Road, Xi'an, Shaanxi Province, 710064, China;
⋆Corresponding author. Email: cyang@ieee.org

ARTICLE HISTORY
Compiled February 13, 2019

ABSTRACT
To develop secure, natural, and effective teleoperation, the perception of the slave plays a key role for the interaction of a human operator with the environment. By sensing slave information, the human operator can choose the correct operation in a process of human-robot interaction. This paper develops an integrated scheme based on a hybrid control and virtual fixture approach for the telerobot. The human operator can sense the slave interaction condition and adjust the master device via the surface electromyographic signal. This hybrid control method integrates proportional-derivative control and variable stiffness control, and involves muscle activation at the same time. It is proposed to quantitatively analyse the human operator's control demand to enhance the control performance of the teleoperation system. In addition, due to unskilful operation and muscle physiological tremor of the human operator, a virtual fixture method is developed to ensure accuracy of operation and to reduce the operation pressure on the human operator. Experimental results demonstrated the effectiveness of the proposed method for the teleoperated robot.

KEYWORDS
Telerobots; variable stiffness; muscle activation; hybrid control; virtual fixture

1. Introduction

Over the last 30 years, the research has focused on the replacement of humans by robots in unknown or dangerous environments. Robots have been widely used in several areas, such as industrial applications, for deep-sea exploration, and for medical service (Bolopion et al., 2013; Chan et al., 2014; Perera et al. , 2014; Zhang J. et al. , 2017). Since then, the telerobot developed into a research hot-spot in the field of robotics.

A typical teleoperated system includes four parts, i.e., the human operator and the master device, the communication channel, a slave device, and its surrounding environment (Li et al. , 2015; Lu et al. , 2017; Yang C. and Wang, X. et al. , 2017). To guarantee the stability and transparency of the teleoperated system, numerous related studies have been developed (Jiang et al., 2016; Yang et al. , 2016). Previously(Li et al.

, 2014; Shi et al. , 2002), the authors assumed that master and slave device were linear models and consequently proposed adaptive control technology to control a teleoperated system with uncertainties of different cases. Yang *et al.* (Yang C. and Wang, X. et al. , 2017) proposed radial basis function neural networks (RBFNNs) with wave variable method to deal with influences of system delay and uncertainties. In (Zhai D. and Xia Y. , 2017), Zhai *et al.* developed a finite time method to deal with problems such as model uncertainties, actuator, and time-varying delay for a nonlinear teleoperated system. Li *et al.* (Li et al. , 2016) combined neural network-based control with the parameter adaptive method to handle both kinematic and dynamic uncertainties. Javier *et al.* developed a haptic assistance method to enhance the tracking performance and human machine interaction of a teleoperation system (Corredor et al., 2017). In (Farooq et al., 2016), the authors presented a state convergence-based control method with a Takagi-Sugeno (TS) fuzzy model for nonlinear teleoperation system. Havoutis *et al.* (Havoutis et al., 2017) developed an integrated method involving optimal control and online learning to accomplish a manipulation task for underwater remotely operated vehicles during supervisory teleoperation. Additionally, Daniel *et al.* proposed a user-controlled variable impedance method with implicit haptic feedback for unstructured environments (Walker et al. , 2010). Panagiotis *et al.* used an EMG signal with a switching regime model as control interface for real-time operation (Artemiadis et al., 2011). In (Ajoudani et al., 2011; Ajoudani A. et al., 2011), the authors introduced a tele-impedance method based on a surface electromyography (sEMG) signal with good manipulation performance for human-robot interaction (HRI).

It is difficult to provide sufficient real time perception for a teleoperation system. Moreover, due to the unskilful operation and muscle physiological tremor of the human operator, the natural performance cannot guarantee secure operation (Li et al. , 2017; Liu et al. , 2014, 2015; Zhao S. et al. , 2017). Thus, it is important to enhance the interaction capability of the teleoperation system. Virtual fixture is an alternative method to improve teleoperation performance. Virtual fixture was first proposed to extract relevant information between the human operator and the remote environment for HRI (Rosenberg, L. B , 1993). In (Fehlberg et al., 2014), a virtual fixture control strategy was presented to improve the manipulation performance of the active handrest. Brian *et al.* developed a derivation of virtual fixtures based on the motion of the instrument in real time for system control(Becker et al., 2013). In (Hong et al., 2016), the authors proposed a forbidden region virtual fixture with robust fuzzy logic controller to improve the human manipulation performance during laparoscopic surgery. A virtual fixture method based on the position error was presented to add an augmentation force on the master device to improve the task quality (Maddahi et al. , 2015). In (Selvaggio et al. , 2016), Selvaggio *et al.* proposed an online virtual fixture and task switching mechanism that utilizes a stereo camera system to provide position information, thus improving teleoperation performance. In (Quintero et al. , 2017), a flexible virtual fixture method with force-vision-based scheme was developed to reduce cognitive load and improve the task performance.

This paper proposes a combined scheme of hybrid control and virtual fixture to improve teleoperation performance. In the proposed hybrid method, muscle activation is introduced to indicate the variable stiffness for the slave in the process of HRI. Combination of the proposed method with the variable stiffness and proportional-derivative (PD) control method can provide a natural and secure interaction for the teleoperation system. Moreover, a virtual fixture method is presented to alleviate the detrimental influences of unskilful operation by the human operator and reduce operation pressure on the human operator. Finally, experimental results have demonstrated

the performance of the proposed method.

The remainder of this paper is structured as follows. In Section 2, the proposed control strategy is developed to improve the system's HRI capability and to enhance the manipulation performance. Experimental results are presented in Section 3 to verify the effectiveness of the presented hybrid control and virtual fixture approach. Section 4 presents the conclusion and future directions.

2. Method

2.1. System description

The teleoperated robot is a novel implement that provides an interaction mode between the human operator and the telerobot, thus enhancing human perception and motion and integrating the human intelligence with the advantages of the robot under long distance constraints.

The block diagram shown in Fig. 1 explains the teleoperation system. The teleoperated robotic system utilizes a master-slave structure and the slave device follows the master motion, operated by the human operator. In this paper, a novel algorithm is developed that involves muscle activation and stiffness control of the human operator with virtual fixture to obtain satisfying performance.

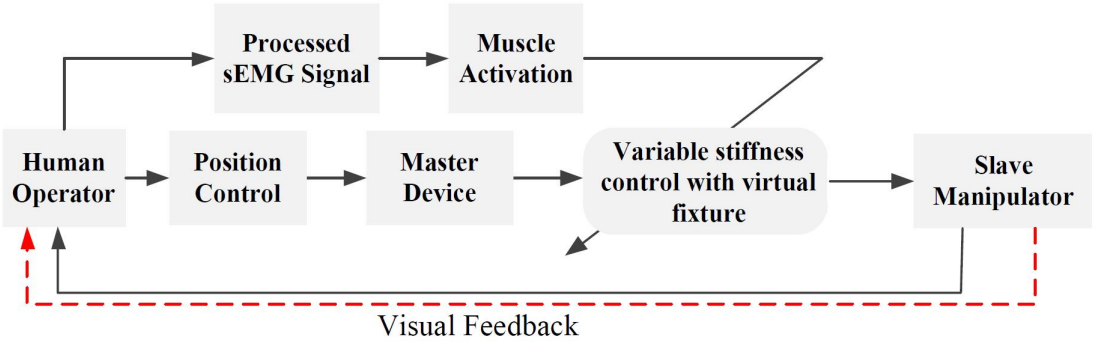

Figure 1. Block diagram of the proposed system.

A schematic diagram and overview of the proposed method with virtual fixture and hybrid control are presented in Fig. 2 and Algorithm 1 . The proposed method is composed of a master side module, slave side module, haptic interface module, and sEMG signal processing module. The master side involves virtual fixture based on position error. PD control and variable stiffness method enables the slave side to provide a force feedback to the haptic device through the haptic interface. The control stiffness with regard to muscle activation can be changed by varying the generated force and haptic force reflection.

2.2. Teleoperation system

The teleoperation system employs a master-slave frame to accomplish the required manipulation task. In general, both master and slave can be extended to a multi-freedom robotic system.

Algorithm 1 Proposed method

1. PD control for the teleoperation system.

$$F_{pd} \leftarrow \widetilde{x}_e \tag{1}$$

F_{pd}: PD controller for the system.
$\widetilde{x}_e$: Deviation between desired and actual trajectory.

2. Variable stiffness control for the teleoperation system.

$$F^{\alpha} \leftarrow K^{\alpha} \tag{2}$$

F^{α}: Force feedback of the slave.
K^{α}: Variable stiffness based on muscle activation.

3. Hybrid control for the teleoperation system.

$$u_1 \leftarrow \widetilde{x}_e, K^{\alpha} \tag{3}$$

u_1: Control law of the slave.

4. Virtual fixture for the teleoperation system.

$$F_{vf} = K_{vf} P_m^e \tag{4}$$

F_{vf}: Generated force based on virtual fixture.
K_{vf}: Matrix of virtual fixture.
P_m^e: Position error of the master.

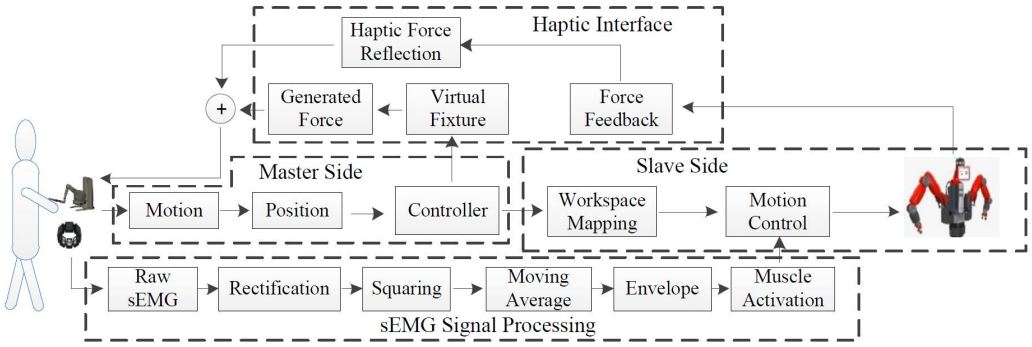

Figure 2. Schematic diagram of the proposed method with virtual fixture and hybrid control.

The dynamics of master and slave are presented as

$$M_m(q_m)\ddot{q}_m + H_m(q_m, \dot{q}_m) = f_m(t) + J_m^T F_h(t) - \tau_m \tag{5}$$

where

$$H_m(q_m, \dot{q}_m) = C_m(q_m, \dot{q}_m)\dot{q}_m + G_m(q_m) \tag{6}$$

$$M_s(q_s)\ddot{q}_s + H_s(q_s, \dot{q}_s) = f_s(t) - J_s^T F_e(t) + \tau_s \tag{7}$$

$$H_s(q_s, \dot{q}_s) = C_s(q_s, \dot{q}_s)\dot{q}_s + G_s(q_s) \tag{8}$$

where $i = m, s$ indicate the master device and the slave device, respectively. $M_i(q_i)$ represents the inertia matrix for the master and the slave. $C_i(q_i, \dot{q}_i)$ represents the Coriolis and Centrifugal force matrix. G_i represents the gravitational force matrix. q_i represents the joint variables. τ_i represents the control inputs. J_i^T represents the transpose of the Jacobian matrix. $H_i(q_i, \dot{q}_i)$ represent the nonlinear coupling terms for the centripetal force, Coriolis force and gravity. $f_m(t)$ and $f_s(t)$ represent the disturbances (Coulomb friction and time-delayed jamming) of master device and slave device, respectively. $F_h(t)$ represents the human operator applied force to the robot. $F_e(t)$ represents the interaction force between the slave and the environment.

- *Property 1.* $M_m(q_m) \in R^{n\times n}$ is a symmetric positive-define matrix.
- *Property 2.* $z^T(\dot{M}_m(q_m) - 2C_m(q_m, \dot{q}_m))z = 0, \forall z \in R^n$.
- *Property 3.* $M_m(q_m)$ is bounded. $G_m(q_m)$ is bounded. It satisfies $\forall q_m, \dot{q}_m \in R^n, \exists K_{cm} \in R > 0$ according to $C_m(q_m, \dot{q}_m)$, so that $\| C_m(q_m, \dot{q}_m) \| \leq K_{cm}|\dot{q}_m|$.

2.3. Control method

The control scheme is shown in Fig. 3. A PD controller and a hybrid method of position controller and stiffness controller are proposed for the master device and the slave device, respectively. As shown, the overall control scheme consists of a PD control module and a variable stiffness control module in Cartesian space.

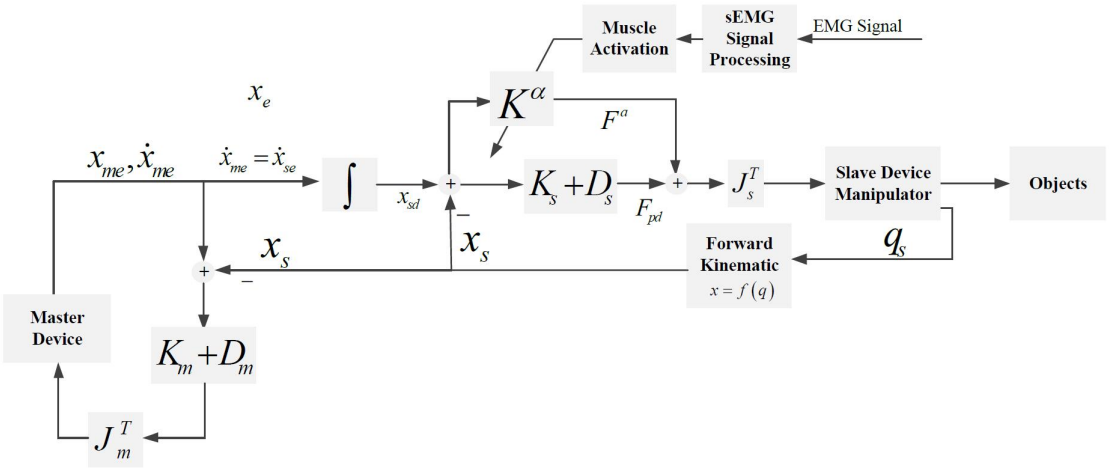

Figure 3. Schematic diagram of the proposed control approach.

2.3.1. PD control of the master

A PD controller is employed for the master and can be defined as

$$\begin{aligned} F_m &= K_m(x_m - x_s) - D_m(\dot{x}_m - \dot{x}_s) \\ &= K_m\widetilde{x}_{me} - D_m\dot{\widetilde{x}}_{me} \end{aligned} \tag{9}$$

where K_m and D_m are positive parameters of the PD controller for the master. $\widetilde{x}_{me} = x_m - x_s$ is the deviation between desired trajectory x_m and the actual trajectory x_s.

2.3.2. Hybrid control of the slave

2.3.2.1. PD Control. As shown in Fig. 3, the PD controller can be represented as

$$\begin{aligned} F_{pd} &= K_s(x_{sd} - x_s) - D_s(\dot{x}_{sd} - \dot{x}_s) \\ &= K_s\widetilde{x}_e - D_s\dot{\widetilde{x}}_e \end{aligned} \tag{10}$$

where K_s and D_s are positive parameters of the PD controller for the slave device. $\widetilde{x}_e = x_{sd} - x_s$ indicates the deviation between desired trajectory x_{sd} and actual trajectory x_s.

2.3.2.2. Variable stiffness control. The human operator can adjust the muscle activation according to the external force applied to the slave device. The trend of muscle activation change is based on the deviation from the force that is exerted by the human operator and the feedback force of the slave manipulator[1].

[1]When this deviation is positive, the human operator will "relax" the hand muscle to obtain a small gain. When the deviation is negative, the muscle will contract to "compensate" for the control gain. Both two modes are reflected by the strength of the sEMG signal.

In this study, the collected sEMG signal u_{emg} can be obtained as

$$u_{emg} = \frac{1}{N}\sum_{i=1}^{N}\sqrt{u_{raw}^2(i)} \tag{11}$$

where u_{raw} are the raw sEMG signals and $i = 1, 2, ..., N$ are the sEMG signal detection channels.

Using a moving average filter yields

$$u(k) = \begin{cases} \frac{1}{k}\sum_{j=0}^{k} u_{emg} & k < W_f \\ \frac{1}{W_f}\sum_{j=k-W_f}^{k} u_{emg} & k > W_f. \end{cases} \tag{12}$$

where W_f represents the size of the moving window. Based on Eqs. (11) and (12), the relationship between the raw sEMG signals u_{raw} and the muscle activation $a(k)$ can be presented as (Yang C. et al. , 2017; Yang C. and Luo, J. et al. , 2017).

$$\alpha^k = \frac{e^{\beta u(k)} - 1}{e^{\beta} - 1} \tag{13}$$

where α represents the muscle activation. $u(k)$ represents the processed sEMG signal. $-3 < \beta < 0$ is a parameter involved in the sEMG signal. Through sEMG signal processing, a linear function that describes stiffness can be represented as

$$K^{\alpha} = (K^{\alpha}_{max} - K^{\alpha}_{min})\frac{(\alpha_i^k - \alpha^k_{max})}{(\alpha^k_{min} - \alpha^k_{max})} + K^{\alpha}_{min} \tag{14}$$

where K^{α}_{max} represents the maximum of K^{α}, and K^{α}_{min} represents the minimum of K^{α}, i.e. $K^{\alpha}_{min} \leq K^{\alpha} \leq K^{\alpha}_{max}$. α^k_{min} and α^k_{max} are the upper and lower bound of the muscle activation, respectively[2]. The variable stiffness parameter K^{α} describes the generation of the optimal stiffness from human operator for slave manipulation. The values of K^{α}_{max} and K^{α}_{min} are devised to rely on experimental experience generated in advance.

According to Eqs. (11)-(14), the variable stiffness control can be defined as

$$F^{\alpha} = K^{\alpha}(x_{sd} - x_s) \tag{15}$$

where $K^{\alpha} > 0$ is the variable stiffness that indicates strength of muscle activation.

In general, the muscle activation of the human operator varies with the manipulation and the external environment during teleoperation. By sensing the information of the remote environment, the human operator can initiate a correct operation/demand

[2]Obtaining the muscle activation is processed by series of treatment steps. The processing procedure includes the following sections: Rectification⇒Squaring⇒Moving average⇒Low pass filter⇒Envelope. The parameters of the muscle activation α^k_{min} and α^k_{max} are determined by a previously conducted pilot experiment.

in HRI. Considering the linear relationship between muscle activation and sEMG signals, the proposed variable stiffness control F^{α} is used to describe the human control operation/demand during teleoperation. By changing the stiffness value K^{α}, the human operator can initiate the correct control of the slave device. Moreover, the control intention of the human operator during teleoperation can be quantitatively analysed via the proposed stiffness control method.

2.3.2.3. Hybrid control. During the process of HRI, the control force F^{r} involves the muscle activation F^{a} and the generated force F_{pd}, as shown in Fig. 3. This can be obtained by Eqs. (10), (15) and (14) as follows:

$$\begin{aligned} F^{r} &= F^{a} + F_{pd} \\ &= \underbrace{K^{\alpha}(x_{sd} - x_{s})}_{F^{a}} + \underbrace{K_{s}(x_{sd} - x_{s}) - D_{s}(\dot{x}_{sd} - \dot{x}_{s})}_{F^{pd}} \\ &= \underbrace{\big((K^{\alpha}_{max} - K^{\alpha}_{min})\frac{(\alpha^{k}_{i} - \alpha^{k}_{max})}{(\alpha^{k}_{min} - \alpha^{k}_{max})} + K^{\alpha}_{min}\big)\widetilde{x}_{e}}_{F^{a}} \\ &\quad + \underbrace{K_{s}\widetilde{x}_{e} - D_{s}\dot{\widetilde{x}}_{e}}_{F^{pd}} \end{aligned} \tag{16}$$

where F^{r} represents the force integrated variable stiffness with PD control based on the Cartesian space. In the variable stiffness control method, variable parameter K^{α} is introduced that reflects the muscle activation necessary to acquire of optimal force in the process of HRI. The proposed controller synthesises the virtue of both feedback and the human operator's factor. This schedule achieved a good realization of the incorporation between human intention and the dynamics of the robots.

The control law of the slave device can be represented as

$$u = J_{s}^{T} F^{r} \tag{17}$$

The control law (17) achieves the hybrid control with regard to position and stiffness in Cartesian space.

2.4. Virtual fixture

When the slave follows the master, the position of end effector of the slave can be defined as

$$P_{s} = (x_{s}, y_{s}, z_{s})^{T} \tag{18}$$

where x_{s}, y_{s}, z_{s} represent the positions in the XYZ coordinate system. The desired trajectory of the slave is

$$P_{sd} = (x_{sd}, y_{sd}, z_{sd})^{T} \tag{19}$$

The joint variables $(q_1^s, q_2^s, \cdots, q_n^s)$ of the slave can be obtained by using inverse kinematics.

The position and desired position of the master are presented as

$$\begin{aligned} P_m &= (x_m, y_m, z_m)^T \\ P_{md} &= (x_{md}, y_{md}, z_{md})^T \end{aligned} \tag{20}$$

where the P_m and P_{md} represent the actual and desired position of the master, respectively.

Thus, the position error of the slave end effector as

$$\begin{aligned} P_s^e &= (x_s^e, y_s^e, z_s^e)^T \\ &= \begin{bmatrix} x_s - x_{sd} \\ y_s - y_{sd} \\ z_s - z_{sd} \end{bmatrix} \end{aligned} \tag{21}$$

For the master device,

$$\begin{aligned} P_m^e &= (x_m^e, y_m^e, z_m^e)^T \\ &= \begin{bmatrix} x_m - x_{md} \\ y_m - y_{md} \\ z_m - z_{md} \end{bmatrix} \end{aligned} \tag{22}$$

where P_m^e is the position error of the master.

The generated force is proportional to the position error of the haptic control, which is presented as

$$F_{vf} = K_{vf} P_m^e \tag{23}$$

where K_{vf} represents the matrix of the virtual fixture which indicates the guiding ability of the virtual fixture.

As shown in Fig. virtual-fixture, when $P_m^e \neq 0$, F_{vf} is either a positive/negative force and leads the master moves as expected.

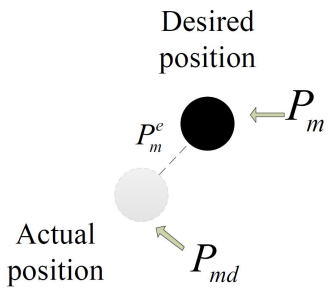

Figure 4. Diagram of the virtual fixture.

2.5. Theoretical analysis

2.5.1. Convergence of tracking error

The generalized tracking error of the slave can be defined as

$$e_{vse} = K_{se}\widetilde{e}_s + \widetilde{\dot{e}}_s \tag{24}$$

where $\widetilde{e}_s = q_s - q_{sd}$, $K_{se} = (K_s + K^{\alpha})D_s^{-1}$. The control input of the slave can defined as

$$\begin{aligned} \tau_s &= -(K_s + K^{\alpha})\widetilde{e}_s - D_s\widetilde{\dot{e}}_s \\ &= -K_{se}D_s\widetilde{e}_s - D_s\widetilde{\dot{e}}_s \\ &= -D_s(K_{se}\widetilde{e}_s + \widetilde{\dot{e}}_s) \\ &= -D_s e_{vse} \end{aligned} \tag{25}$$

Based on (25), (7) can be represented as

$$M_s\dot{e}_{vse} + C_s e_{vse} + G_s + M_s\dot{q}_{sv} + C_s q_{sv} = f_s(t) - J_s^T F_e(t) + \tau_s \tag{26}$$

where $q_{sv} = \dot{q}_{sd} - K_{se}\widetilde{e}_s$.

Combining (25) and (26),

$$M_s\dot{e}_{vse} + C_s e_{vse} + D_s e_{vse} = f_s(t) - J_s^T F_e(t) - G_s + M_s\dot{q}_{sv} - C_s q_{sv} \tag{27}$$

According to (Yang C. and Wang, X. et al. , 2017), the uncertain dynamics of the slave device with the input z_s can be represented as

$$f(z_s) = f_s(t) - J_s^T F_e(t) - G_s + M_s\dot{q}_{sv} - C_s q_{sv} \tag{28}$$

In this paper, the dynamics of the slave device are assumed to be available for trajectory tracking. Thus, (27) can be rewritten as:

$$M_s\dot{e}_{vse} + C_s e_{vse} + D_s e_{vse} = 0 \tag{29}$$

and

$$M_s\dot{e}_{vse} = -(C_s + D_s)e_{vse} \tag{30}$$

Proof. Consider a Lyapunov function as below

$$V = \frac{1}{2}e_{vse}^T M_s e_{vse} \tag{31}$$

Using the derivation method yields

$$\dot{V} = \frac{1}{2} e_{vse}^T \dot{M}_s e_{vse} + e_{vse}^T M_s \dot{e}_{vse} \tag{32}$$

Based on (30), one have

$$\begin{aligned} \dot{V} &= \frac{1}{2} e_{vse}^T \dot{M}_s e_{vse} - e_{vse}^T C_s \dot{e}_{vse} - e_{vse}^T D_s \dot{e}_{vse} \\ &= -e_{vse}^T D_s \dot{e}_{vse} < 0 \end{aligned} \tag{33}$$

This results in:

$$\int_{t0}^{t} \dot{V} dt = V(t) - V(0) = \int_{t0}^{t} (-e_{vse}^T D_s \dot{e}_{vse}) dt < 0 \tag{34}$$

Therefore, $\dot{V}$ is negative definite. When $t \longrightarrow \infty$, $e_{vse} \in L_2 \cap L_\infty$, and $\dot{e}_{vse} \in L_\infty$, e_{vse} can be asymptotically converged to 0 (Zhou Q. et al. , 1993).

□

2.5.2. Stability analysis

Proof. Consider a Lyapunov function as below

$$V_1 = \frac{1}{2} q_m^T M_m \dot{q}_m + \frac{1}{2} \widetilde{e}_m^T M_m \widetilde{e}_m + \frac{1}{2} e_{vse}^T M_s e_{vse} \tag{35}$$

where $\widetilde{e}_m = q_m - q_{md}$.

According to Eq. (33), we have

$$\dot{V}_1 = \dot{x}_{me}^T F_h - \dot{x}_s^T F_e - \dot{q}_m^T D_m \dot{q}_m + \dot{V} \tag{36}$$

It can be assumed that the human operator and the external environment are passive (Yang C. and Wang, X. et al. , 2017). Then, we obtain

$$\begin{cases} \int_0^t \dot{x}_{me}^T (-F_h) dt \geq V_{mh}(t) - V_{mh}(0) \\ \int_0^t \dot{x}_d^T F_e dt \geq V_{se}(t) - V_{se}(0) \end{cases} \tag{37}$$

where $V_{mh}(t)$ and $V_{se}(t)$ are bounded.

According to Eqs. (33) and (37), we obtain

$$V_1(t) - V_1(0) \leq \int_0^t (\dot{x}_{me}^T F_h - \dot{x}_s^T F_e) dt + \int_0^t (\dot{V} - \dot{q}_m^T D_m \dot{q}_m) dt \tag{38}$$

which can guarantee the boundedness of V_1.

The proof is completed.

□

3. Experimental Results

3.1. Experimental Setup

To demonstrate the performance of the proposed integrated algorithm, an experimental platform was built as shown in Fig. 5.

- *Hardware equipment.* The experimental hardware equipment consists of the Touch X, the simulated Baxter robot, and the MYO armband.
- *Software environment.* The software environment includes the MATLAB software, Visual Studio 2013 (VS 2013), and the Windows 7 operation system.
- *Experimental Parameters.* For the experiments, a PD controller is used to control the master. An integrated controller is used to control the slave. The experimental parameters of the master are set as follows: PD controller parameters: $K_m = 50$ and $D_m = 30$; virtual fixture related parameter $K_{vf} = 20$. The following experimental parameters of the slave are set: PD controller parameters of $K_s = 50$ and $D_s = 30$, the parameter of the muscle activation $\beta = -0.6891$.

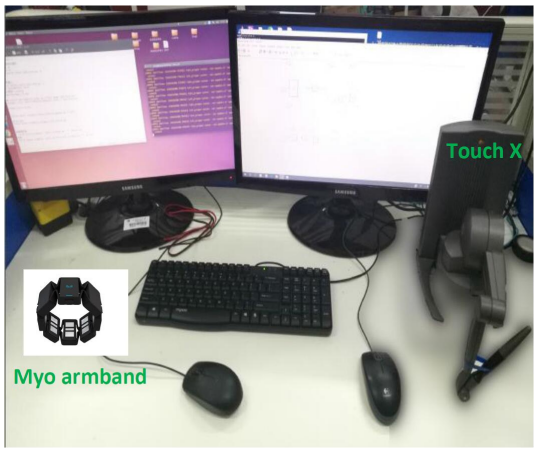

Figure 5. Experimental setup.

3.2. Experimental evaluation

To evaluate the effectiveness of the proposed approach, the root mean squared error (RMSE) was used which is defined as follows:

$$RMSE = \sqrt{\frac{\sum_{i=0}^{N-1}(y(i) - \hat{y}(i))^2}{N}} \tag{39}$$

where $y(i)$ represents the master trajectory and $\hat{y}(i)$ represents the slave trajectory.

3.3. Results

3.3.1. Tracking experiment

Figs. 6-9 show the tracking performance when the PD control mode in X/Y/Z directions is used. The solid red lines indicate the tracking performance of the master device. The dashed black lines are the trajectories of the slave device. As shown in Figs. 6-8, the slave can not follow the master in 0-5 s, but it can preferably follow the master after 5 s in the X/Z directions except for the Y direction. The result of tracking error in PD control is shown in Fig. 9.

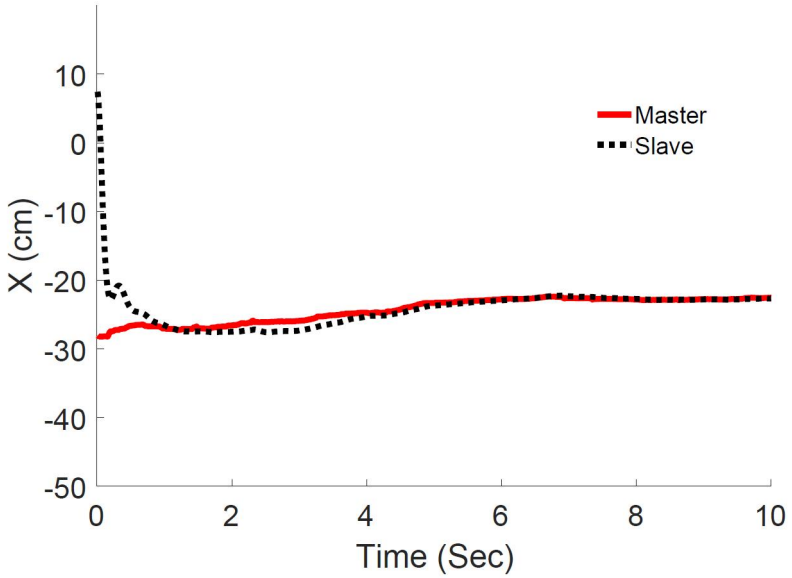

Figure 6. X-Direction trajectory with PD control.

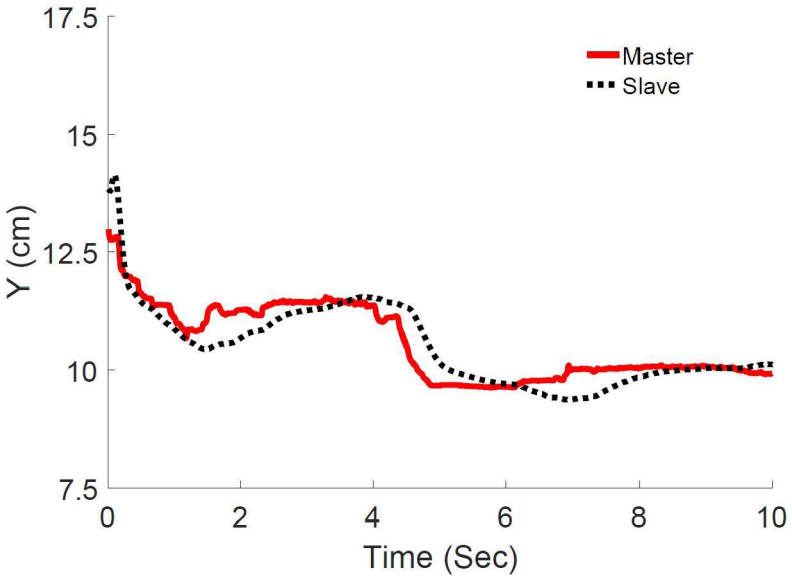

Figure 7. Y-Direction trajectory with PD control.

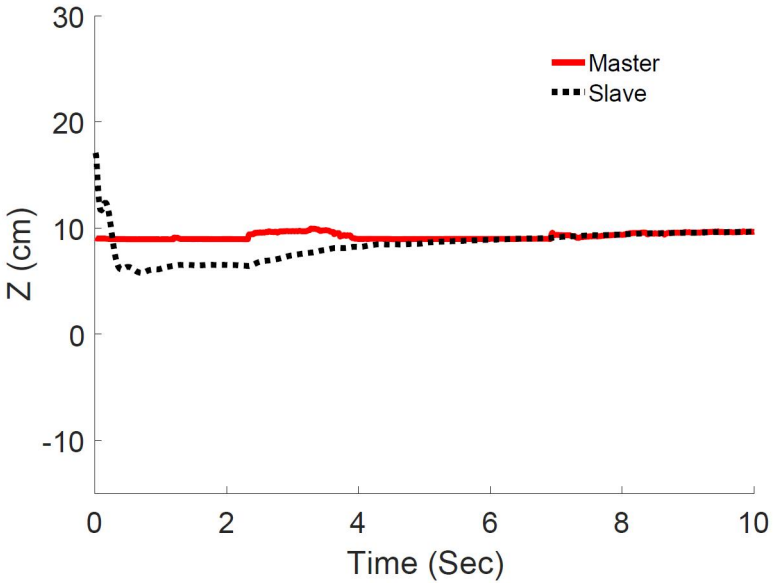

Figure 8. Z-Direction trajectory with PD control.

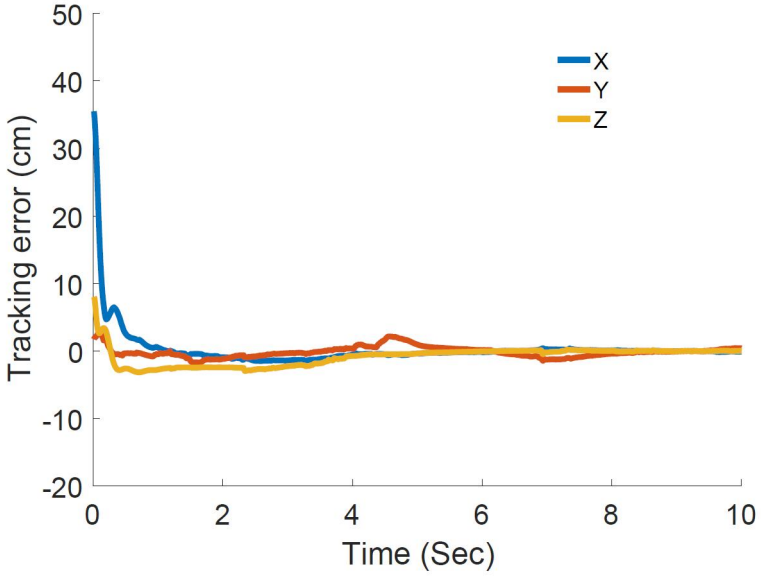

Figure 9. Tracking error with PD control.

.

The results of tracking experiment in hybrid control mode are shown in Figs. 10-13. The solid red lines indicate the tracking performance of the master device. The dashed black lines show the trajectories of the slave device. In Figs. 10-12, the trajectories of the slave do not match the tracking the master in 0-3 s due to different initial positions in the task space. However, the slave almost exactly tracked the trajectories of the master during the last 3-7 s. The tracking error of the slave is depicted in Fig. 13. Compared to the PD control, the error of the tracking trajectory is smaller in case of the hybrid control mode, and the hybrid control mode achieves better performance in trajectory tracking experiments.

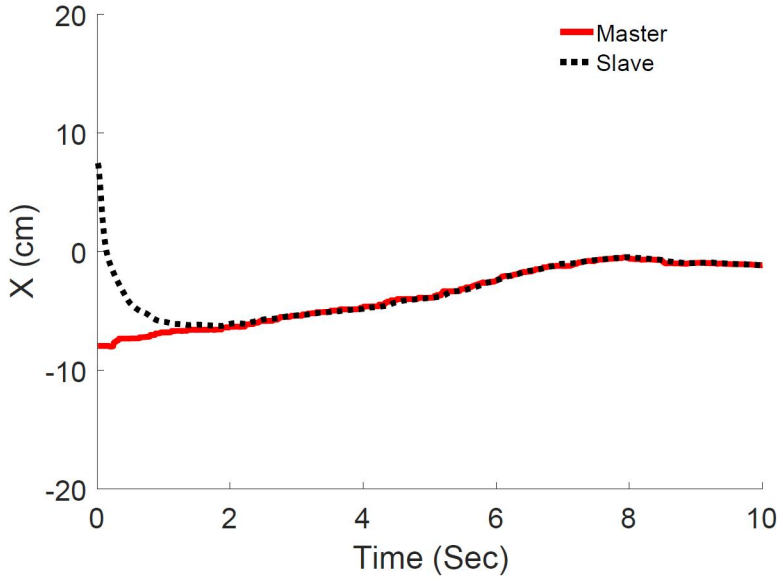

Figure 10. X-Direction trajectory with hybrid control.

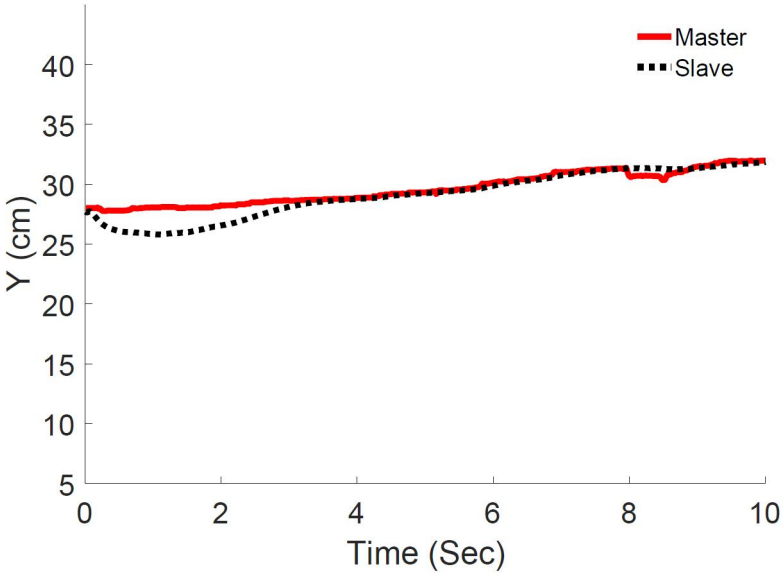

Figure 11. Y-Direction trajectory with hybrid control.

Table 1. Comparisons of tracking performance between PD control and hybrid control: root mean square error (RMSE).

Control Method	PD Control	Hybrid Control
X (cm)	0.0176	0.0108
Y (cm)	0.0093	0.0081
Z (cm)	0.0173	0.0160

Table 1 shows that the tracking errors of the hybrid control are 0.0108, 0.0081, and 0.0160 in X, Y, and Z directions, respectively. However, the tracking errors of

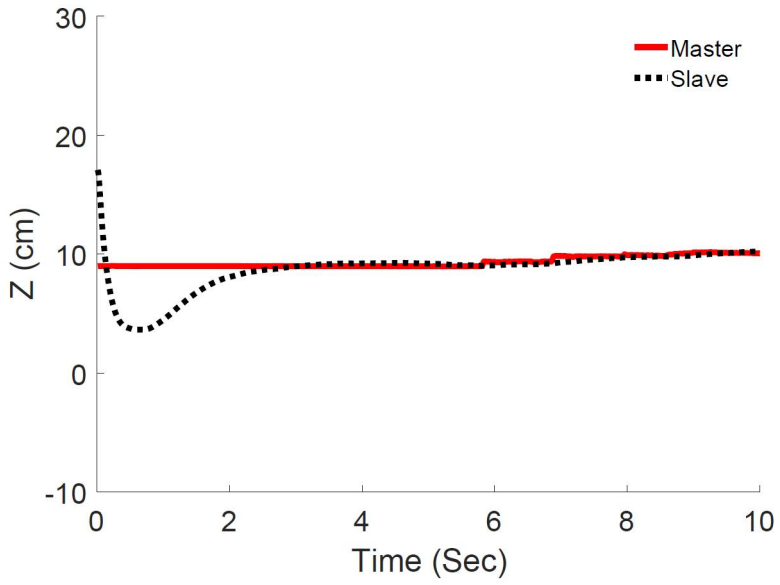

Figure 12. Z-Direction trajectory with hybrid control.

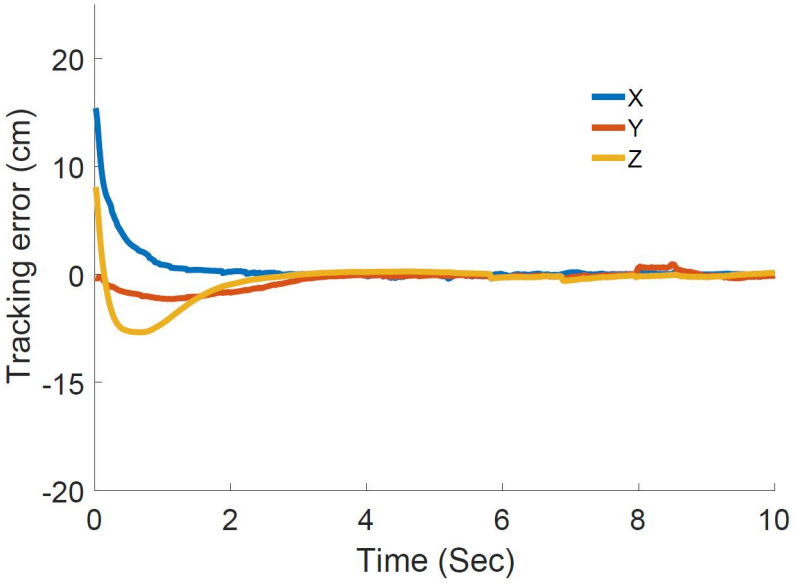

Figure 13. Tracking error with hybrid control.

the PD control are 0.0176, 0.0093, and 0.0173 in X, Y, and Z directions, respectively. The values of RMSE are smaller in the integrated control mode compared to the PD control mode. Consequently, the tracking performance of the proposed hybrid control method is superior to that of the PD control method.

3.3.2. Virtual fixture experiment

Based on the tracking experiment, a typical trajectory of the slave device end-effector in the Cartesian space is presented to verify the performance of the proposed method using virtual fixture. In this experiment, the trajectory error had to be smaller com-

pared to that of the tracking experiment.

Figs. 14-18 show the trajectory performance in the operation space. The solid red lines indicate the tracking performance of the master device. The dashed black lines are the trajectories of the slave device. As shown in Figs. (14)-(15), the slave can precisely follow the master all the time. As shown in Figs. (16)-(17), the slave can also almost track the master by using virtual fixture in comparison to Figs. (14)-(15). The generated force by using virtual fixture is shown in Fig. (18). As shown in Fig. (14) and Fig. (16), the completion time of the task in case of virtual fixture is below that for the case of without virtual fixture.

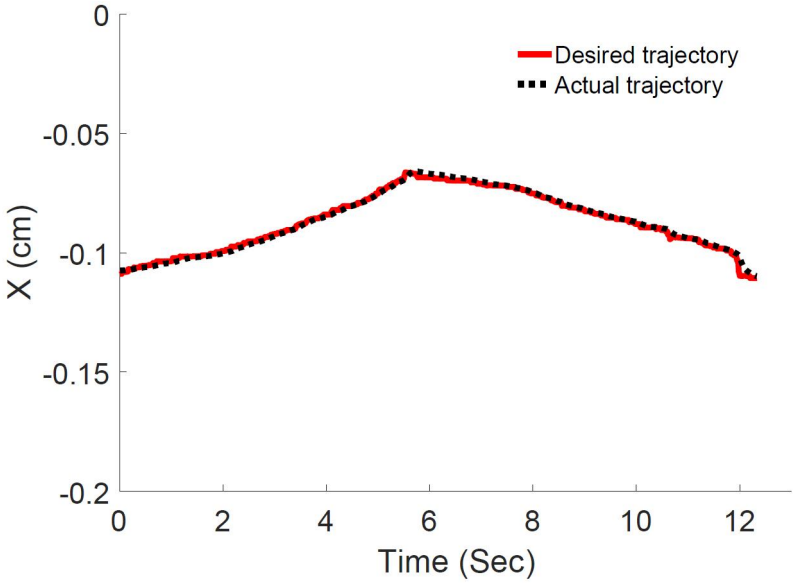

Figure 14. Position tracking without virtual fixture.

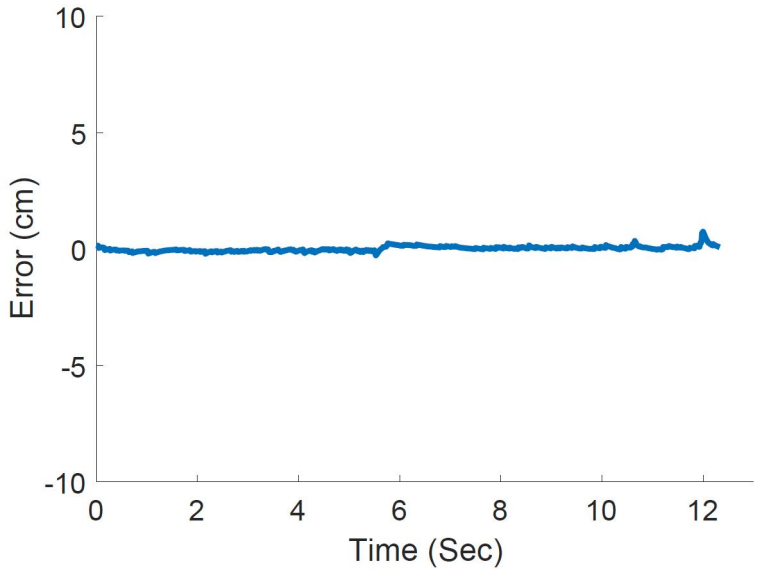

Figure 15. Tracking error without virtual fixture.

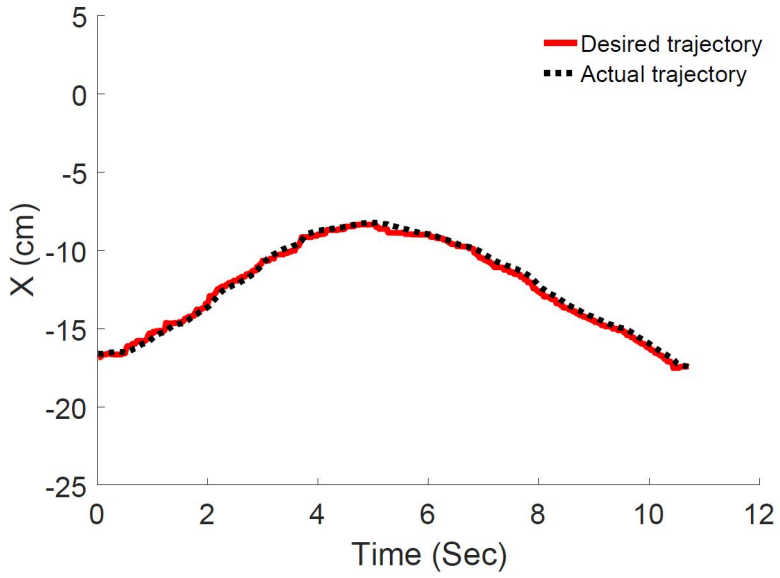

Figure 16. Position tracking with virtual fixture.

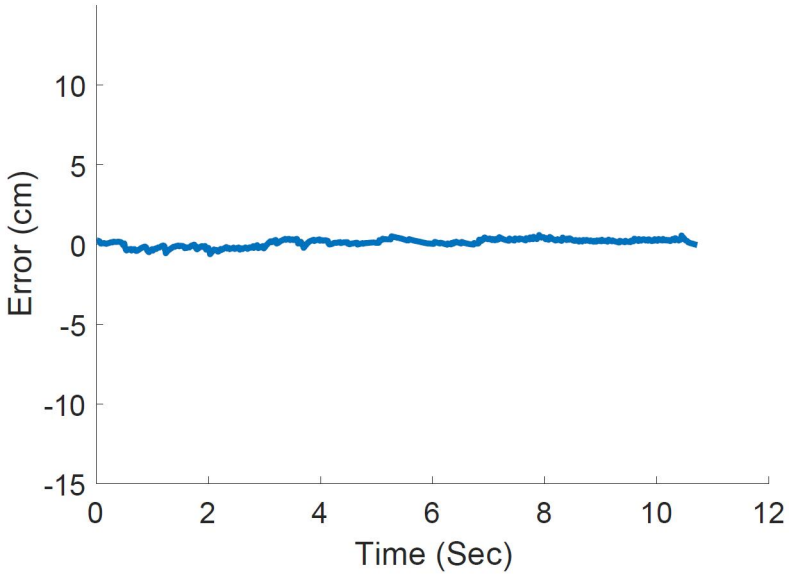

Figure 17. Tracking error with virtual fixture.

Table 2. Performance comparisons between with and without virtual fixture control: root mean square error and completion time of the task.

Method	Tracking Error (cm)	Completion Time (s)
without virtual fixture	0.0011	12.33
virtual fixture	0.0025	10.72

The experimental results observation as shown in Table 2, indicate that the RMSE of

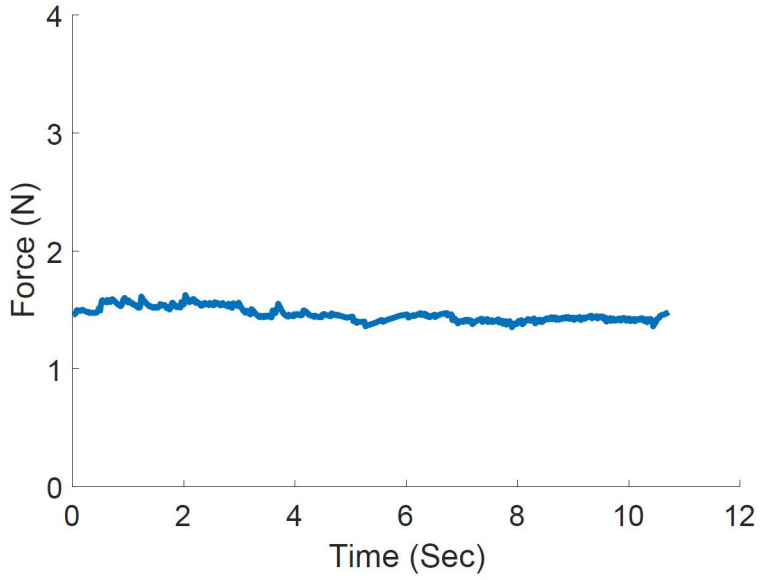

Figure 18. Generated force by using virtual fixture.

the tracking trajectory between the cases with and without virtual fixture are 0.0011 and 0.0025, respectively. It should be noted that the RMSE in the virtual fixture experiment is smaller than the RMSE in the tracking experiment. The time spend on the trajectory task without virtual fixture is 12.33 s, while the completion time is 10.72 s in case of virtual fixture.

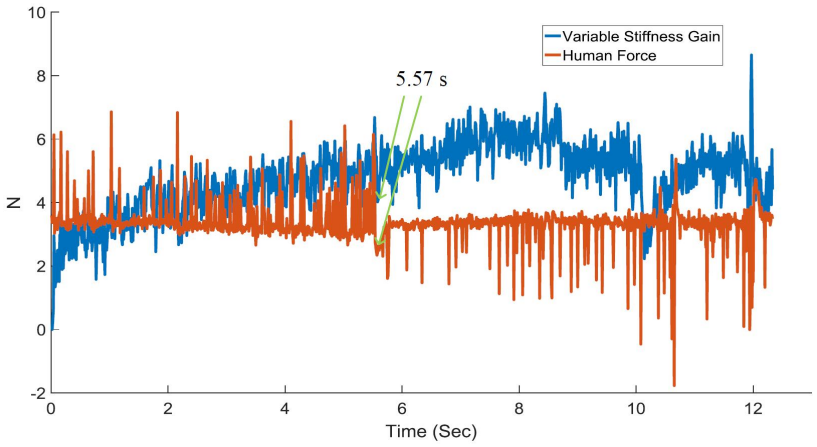

Figure 19. Performance of variable stiffness gain and human force without virtual fixture.

Figs. 19-20 show the trajectories of the variable stiffness gain K^{α} and the human force. The curves of K^{α} and human force vary with the position trajectory. The values of K^{α} and human force are increased under both conditions of with and without virtual fixture. It can be concluded that the variable stiffness gain K^{α} is positively correlated to the human force.

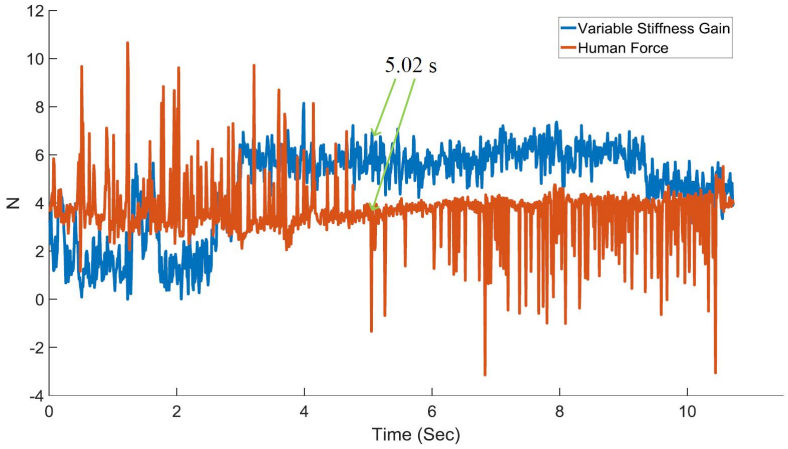

Figure 20. Performance of variable stiffness gain and human force by using virtual fixture.

4. Conclusion

This paper proposes a novel scheme that combines hybrid control with virtual fixture and achieves a good manipulation performance of the telerobot. The hybrid control method integrated with both PD control and variable stiffness control and the proposed method could provide both natural and secure interaction for the human operator by adjusting their hand muscle activation. Based on the hybrid control structure, a virtual fixture method was presented to improve the manipulation performance of the human operator. The experimental results verified the performance of the proposed method. In future, more human physiological informations will be introduced, i.e. electroencephalogram (EEG) and electro-oculogram (EOG) to enhance both the perception and interaction experience of the human operator for the teleoperation.

Acknowledgement(s)

This work was partially supported by Engineering and Physical Sciences Research Council (EPSRC) under Grant EP/S001913/1and in part by the National Natural Science Foundation of China under Grant No. 61803039.

References

Ajoudani, A. and Tsagarakis, N. G and Bicchi, A. (2011). Tele-impedance: Preliminary results on measuring and replicating human arm impedance in tele operated robots. *Robotics and Biomimetics (ROBIO), 2011 IEEE International Conference on.* 216–222.

Ajoudani, A. and Tsagarakis, N. G and Bicchi, A. (2011). Tele-Impedance based teleoperation: Peg-in-hole experimental results. *Robotics and Biomimetics (ROBIO), 2011 IEEE International Conference on.* 2239–2240.

Artemiadis, P. K and Kyriakopoulos, K. J. (2011). A switching regime model for the EMG-based control of a robot arm. *IEEE Transactions on Systems, Man, and Cybernetics, Part B (Cybernetics).* *41*(1) 53–63.

Becker, B. C and MacLachlan, R. A and Lobes, L. A and Hager, G. D and Riviere, C. N.

(2013). Vision-based control of a handheld surgical micromanipulator with virtual fixtures. *IEEE Transactions on Robotics. 29*(3) 674–683.

Bolopion, A. and Régnier, S. (2013). A review of haptic feedback teleoperation systems for micromanipulation and microassembly. *IEEE Transactions on automation science and engineering. 10*(3) 496–502.

Chan, L. and Naghdy, F. and Stirling, D. (2014). Application of adaptive controllers in teleoperation systems: A survey. *IEEE Transactions on Human-Machine Systems. 44*(3) 337–352.

Corredor, J. and Sofrony, J. and Peer, A. (2017). Decision-making model for adaptive impedance control of teleoperation systems. *IEEE transactions on haptics. 10*(1) 5–16.

Farooq, U. and Gu, J. and El-Hawary, M. and Asad, M. U. and Abbas, G. (2016). Fuzzy model based bilateral control design of nonlinear tele-operation system using method of state convergence. *IEEE Access. 4* 4119–4135.

Fehlberg, M. A and Nisky, I. and Doxon, A. J and Provancher, W. R (2014). Improved active handrest performance through use of virtual fixtures. *IEEE Transactions on Human-Machine Systems. 44*(4) 484–498.

Haddadi, A. and Razi, K. and Hashtrudi-Zaad, K. (2015). Operator Dynamics Consideration for Less Conservative Coupled Stability Condition in Bilateral Teleoperation. *IEEE/ASME Transactions on Mechatronics. 20*(5) 2463–2475.

Havoutis, I. and Calinon, S. (2017). Supervisory teleoperation with online learning and optimal control. *Proc. IEEE Intl Conf. on Robotics and Automation (ICRA), Singapore.*

Hong, M. and Rozenblit, J. W (2016). A haptic guidance system for Computer-Assisted Surgical Training using virtual fixtures. *Systems, Man, and Cybernetics (SMC), 2016 IEEE International Conference on. 0*02230–002235.

Jiang, Y. and Yang, C. and Ma, H. (2016). A Review of Fuzzy Logic and Neural Network Based Intelligent Control Design for Discrete-Time Systems. *Discrete Dynamics in Nature and Society,2016,(2016-3-31). 2016*(4) 1–11.

Lawrence, D. A (1993). Stability and transparency in bilateral teleoperation. *IEEE Transactions on Robotics and Automation. 3*(5) 1316–1321.

Li, Z. and Xia, Y. and Wang, D. and Zhai, D. and Su, C. and Zhao, X. (2016). Neural network-based control of networked trilateral teleoperation with geometrically unknown constraints. *IEEE transactions on cybernetics. 45*(6) 1051–1064.

Li, Z. and Kang, Y. and Xiao, Z. and Song, W. (2017). Human–robot coordination control of robotic exoskeletons by skill transfers. *IEEE Transactions on Industrial Electronics. 64*(6) 5171–5181.

Li, Z. and Xia, Y. and Sun, F. (2014). Adaptive fuzzy control for multilateral cooperative teleoperation of multiple robotic manipulators under random network-induced delays. *IEEE Transactions on Fuzzy Systems. 22*(2) 437–450.

Li, Z. and Xia, Y. and Su, C. (2015). Intelligent networked teleoperation control. *Springer. 2015.*

Liu, Z. and Mao, C. and Luo, J. and Zhang, Y. and Chen, CL P. (2014). A three-domain fuzzy wavelet network filter using fuzzy PSO for robotic assisted minimally invasive surgery. *Knowledge-Based Systems. 2014*(66) 13–27.

Liu, Z. and Luo, J. and Wang, L. and Zhang, Y. and Philip C., CL and Chen, X. (2015). A time-sequence-based fuzzy support vector machine adaptive filter for tremor cancelling for microsurgery. *International Journal of Systems Science. 46*(6) 1131–1146.

Lu, Z. and Huang, P. and Liu, Z. (2017). Predictive Approach for Sensorless Bimanual Teleoperation under Random Time Delays with Adaptive Fuzzy Control. *IEEE Transactions on Industrial Electronics. 65*(3) 2439–2448.

Maddahi, Y. and Zareinia, K. and Sepehri, N. (2015). An augmented virtual fixture to improve task performance in robot-assisted live-line maintenance. *Computers and Electrical Engineering. 43* 292–305.

Perera, G. A. and Abeykoon, AM H. S (2014). Review on bilateral teleoperation with force, position, power and impedance scaling. *Information and Automation for Sustainability (ICIAfS), 2014 7th International Conference on. 1*–7.

Quintero, C. P. and Dehghan, M. and Ramirez, O. and Ang, M. H and Jagersand, M. (2017). Flexible virtual fixture interface for path specification in tele-manipulation. *Robotics and Automation (ICRA), 2017 IEEE International Conference on. 5*363–5368.

Rosenberg, L. B (1993). Virtual fixtures: Perceptual tools for telerobotic manipulation. *Virtual Reality Annual International Symposium, 1993., 1993 IEEE.* 76–82.

Selvaggio, M. and Notomista, G. and Chen, F. and Gao, B. and Trapani, F. and Caldwell, D. (2016). Enhancing bilateral teleoperation using camera-based online virtual fixtures generation. *Intelligent Robots and Systems (IROS), 2016 IEEE/RSJ International Conference on. 1*483–1488.

Shi, M. and Tao, G. and Liu, H. (2002). Adaptive control of teleoperation systems. *Journal of X-Ray Science and Technology. 10*(1-2) 37–57.

Tugal, H. and Carrasco, J. and Falcon, P. and Barreiro, A. (2017). Stability Analysis of Bilateral Teleoperation With Bounded and Monotone Environments via ZamesFalb Multipliers. *IEEE Transactions on Control Systems Technology. 25*(4) 1131–1344.

Walker, D. S and Wilson, R. P and Niemeyer, G. (2010). User-controlled variable impedance teleoperation. *Robotics and Automation (ICRA), 2010 IEEE International Conference on. 5*352–5357.

Yang, C. and Jiang, Y. and Li, Z. and He, W. and Su, C. (2016). Neural Control of Bimanual Robots with Guaranteed Global Stability and Motion Precision. *IEEE Transactions on Industrial Informatics. 13*(3) 1162–1171.

Yang, C. and Zeng, C. and Liang, P. and Li, Z. and Li, R. and Su, C. (2017). Interface Design of a Physical Human-Robot Interaction System for Human Impedance Adaptive Skill Transfer. *IEEE Transactions on Automation Science and Engineering. 15*(1) 329–340.

Yang, C. and Luo, J. and Pan, Y. and Liu, Z. and Su, C. (2017). Personalized Variable Gain Control With Tremor Attenuation for Robot Teleoperation. *IEEE Transactions on Systems Man and Cybernetics: Systems. 48*(10) 1759–1770.

Yang, C. and Wang, X. and Li, Z. and Li, Y. and Su, C. (2017). Teleoperation control based on combination of wave variable and neural networks. *IEEE Transactions on Systems Man and Cybernetics: Systems. 47*(8) 2125–2136.

Zhai, D. and Xia, Y. (2017).Finite-time control of teleoperation systems with input saturation and varying time delays. *IEEE Transactions on Systems Man and Cybernetics: Systems. 47*(7) 1522–1534.

Zhang, J. and Li, W. and Yu, J. and Zhang, Q. and Cui, S. and Li, Y. and Li, S. and Chen, G. (2017). Development of a virtual platform for telepresence control of an underwater manipulator mounted on a submersible vehicle. *IEEE Transactions on Industrial Electronics. 64*(2) 1716–1727.

Zhao, S. and Li, Z. and Cui, R. and Kang, Y. and Sun, F. and Song, R. (2017). Brain–machine interfacing-based teleoperation of multiple coordinated mobile robots. *IEEE Transactions on Industrial Electronics. 64*(6) 5161–5170.

Zhou, Q. and Xu, J. and TP, L. (1993). Globally stable adaptive controller of robot manipulators. *TENCON'93. Proceedings. Computer, Communication, Control and Power Engineering. 1993 IEEE Region 10 Conference on. 4* 901–93.